Nanoscale Advances

ROYAL SOCIETY OF CHEMISTRY

PAPER

View Article Online
View Journal | View Issue

Cite this: *Nanoscale Adv.*, 2025, **7**, 5221

Sulfonic acid grafted on silica-shell silver nanoparticles as a novel catalyst for the preparation of pyrimido[4,5-*b*]quinolines†

Seyede Elaheh Ghafouri,[a] Hamid Goudarziafshar*[a] and Ahmad Reza Moosavi-Zare *[b]

Received 23rd April 2025
Accepted 3rd July 2025

DOI: 10.1039/d5na00393h

rsc.li/nanoscale-advances

In this research, Ag@SiO_2 nanoparticles were prepared by a sol–gel method (a wet chemical method) at room temperature. The nanoparticles were functionalized by chlorosulfonic acid to introduce acidic sites on the surface to obtain sulfonic acid grafted on silica-coated silver nanoparticles (Ag@SiO_2–SO_3H). Ag@SiO_2–SO_3H was identified and characterized by FT-IR, DLS, ZP, FE-SEM, EDX-mapping, TEM, XRD, BET, BJH and TGA analyses. Ag@SiO_2–SO_3H performed well as a reusable catalyst for the multi-component synthesis of pyrimido[4,5-*b*]quinoline derivatives with high efficiency and satisfactory results.

Introduction

Heterocyclic compounds with pyrimidine, pyrimidoquinoline, and quinolone moieties have attracted attention in chemistry and pharmaceuticals because of their significant biological properties. One of these important biological classes of compounds is the pyrimido[4,5-*b*]quinolines, which exhibit various biological activities including antifungal,[1] antimalarial,[2] anticancer,[3,4] antiviral,[5] antihistaminic,[6] anti-oxidant,[7] anti-microbial,[7] and anti-inflammatory properties.[7,8]

Some important pyrimido[4,5-*b*]quinolone derivatives were prepared by the three-component reaction of an aldehyde with dimedone and 6-amino-1,3-dimethyluracil.[7] Multi-component synthesis is an important protocol in green chemistry that has recently been attracted much attention because it allows the preparation of products in one step without generating side products during the reaction; moreover, this approach prevents the waste of energy, materials, and solvents, shortens reaction times, and increases reaction efficiency.[9–15]

Various catalysts have been used for the multi-component preparation of pyrimido[4,5-*b*]quinolones, including SBA-15/PrN($CH_2PO_3H_2$)$_2$,[16] trityl chloride (TrCl),[17] nano-[Fe_3O_4@SiO_2/*N*-propyl-1-(thiophene-2-yl)ethanimine][$ZnCl_2$],[18] [TSSECM],[19] *N*,*N*-diethyl-*N*-sulfoethanaminium chloride,[20] [H_2-DABCO][ClO_4]$_2$,[21] Fe_3O_4@cellulose sulfuric acid,[22] glycolic acid-supported cobalt ferrite,[23] nano-[Fe_3O_4@-SiO_2@R-$NHMe_2$][H_2PO_4],[24] [bmim]Br,[25] nanocrystalline MgO,[26] agar-entrapped sulfonated DABCO,[27] [C_4(DABCO)$_2$]·2OH,[28] DABCO,[29] cellulose sulfuric acid,[30] nano-[Fe_3O_4@SiO_2@BDIL],[31] $Cs_{2.3}H_{0.7}PW_{10}Mo_2O_{40}$,[32] Fe_3O_4@SiO_2–SO_3H,[33] DABCO-based ionic liquid,[34] nano-[Cu–$4C_3$NSP](Cl)$_2$,[35] [Fe_3O_4@SiO_2@RNMe_2–SO_3H][CF_3CO_2],[36] GO/Fe_3O_4@PTRMS@BDSA@SO_3H,[37] TiO_2/porous carbon nanocomposite,[38] $RuCl_3 \cdot xH_2O$,[39] and triethylbenzylammonium chloride (TEBAC)[40] are some catalyst which recently used and reported for the preparation of pyrimido[4,5-*b*]quinolines. Given the important biological activities exhibited by pyrimido[4,5-*b*]quinoline derivatives, finding new methods for the synthesis of these compounds remains necessary.

Recently, various supported acidic catalysts have been introduced as catalysts in organic transformations. Some catalysts with sulfonic acid moieties were designed and used in reactions owing to their ease of use compared to common inorganic acids in organic reactions. Silica,[41] mesoporous compounds,[42] silica-coated magnetite nanoparticles,[43] inorganic materials,[44] organic materials[45–47] and ionic liquids[48–50] are examples of supports that are used for the preparation of supported or grafted sulfonic acid catalysts.

Silver nanoparticles are used as antimicrobial agents, biosensors, composite fibers, cosmetics, detergents, and electronic components due to their unique properties. In addition, they have attracted the attention of researchers in the fields of medical imaging, nanocomposites, filters, drug delivery, and biolabeling.[51] Ag@SiO_2 has also been applied as a catalyst for various transformations such as low-temperature CO oxidation,[52,53] benzene combustion,[54] redox reactions on surfaces,[55] oxidative dehydrogenation of methanol,[56] reduction of mixtures of 4-nitrophenol (4-NP) and rhodamine-B (Rh-B),[57] decomposition of ozone,[58] selective hydrogenation of acetylene,[59] hydrogenation of 4-nitrophenol,[60] diethyl oxalate hydrogenation to ethyl glycolate,[61] hydrogenation of nitrobenzene,[62] reduction of methylene blue,[63] semi-hydrogenation of dimethyl glycolate,[64]

[a]*Department of Chemical Engineering, Hamedan University of Technology, Hamedan, 65155, Iran. E-mail: , hamid_gafshar@yahoo.com*

[b]*Chemistry Department, College of Sciences, Shiraz University, Shiraz 71946-84795, Iran. E-mail: moosavizare@yahoo.com*

† Electronic supplementary information (ESI) available. See DOI: https://doi.org/10.1039/d5na00393h

hydrogenation of dimethyl oxalate to methyl glycolate[65] and preparation of methyl glycolate through hydrogenation of dimethyl oxalate.[66] Moreover, catalysts have been designed using silver nanoparticles such as $Ag/SiO_2–Al_2O_3$,[67] $Ag/SiO_2–CoFe_2O_4$,[68] $Pd–Ag/SiO_2$,[69] $Ni–Ag/SiO_2$ (ref. 70) and $Cu@Ag/SiO_2$ (ref. 71) to catalyze various chemical reactions.

Considering the above context, in the present work, silica-coated silver nanoparticles were used to prepare sulfonic acid supported on silica-coated silver nanoparticles ($Ag@SiO_2–SO_3H$) as a heterogeneous catalyst for the efficient multi-component synthesis of pyrimido[4,5-*b*]quinolines (Scheme 1).

Experimental

Materials and methods

All chemicals were purchased from Fluka or Merck Chemical Companies. Known products were identified by comparison of their melting points and spectral data with those reported in the literature. The progress of the reactions was monitored by TLC using silica gel SIL G/UV 254 plates. ^{1}H (250 MHz) and ^{13}C NMR (62.5 MHz) spectra of the products were recorded with a Bruker Avance DPX FT-NMR spectrometer (δ in ppm). Melting points were measured with a Büchi B-545 apparatus in open capillary tubes. Fourier transform infrared (FT-IR) spectra of the products were recorded with a PerkinElmer Spectrum 65 FT-IR Spectrometer. Dynamic light scattering (DLS) analysis of the catalyst was conducted with a HORIBA, SZ-100 series nanoparticle analyzer. The size and morphology of the catalyst particles were studied using transmission electron microscopy (TEM) with a TEM Philips EM 208S device. The absorption, desorption and porosity of the samples were measured with a Belsorp-mini II device.

Procedure for the synthesis of $Ag@SiO_2–SO_3H$

Cetyltrimethylammonium bromide (CTAB) (0.044 mmol, 0.016 g) was dissolved in deionized water (24 mL) under stirring at 40–50 °C and then silver nitrate (0.1 mmol, 0.0169 g) and ascorbic acid (0.1 mmol, 0.0176 g) were added (the color of the solution darkened while stirring because of the reduction of Ag^+ to Ag^0). Solid NaOH (0.2 mmol, 0.008 g) was added under stirring, then tetraethyl orthosilicate (TEOS) (0.47 mmol, 0.0975 g) and ethanol (5 mL) were added dropwise over three hours under stirring at room temperature. After 96 hours, silica-coated silver nanoparticles ($Ag@SiO_2$) were obtained as a sediment, which was separated and dried. The $Ag@SiO_2$ (1 g) was then added to dichloromethane (20 mL) and subjected to ultrasound irradiation for 20 min to obtain a uniform mixture that was placed in an ice–water bath. Chlorosulfonic acid (97%) (1.5 mL) was added dropwise and the mixture was stirred for 2 hours to prepare the catalyst. The main catalyst ($Ag@SiO_2–SO_3H$) was washed several times with dichloromethane and dried in an oven at 100 °C for 24 hours.

General method for the synthesis of pyrimido[4,5-*b*]quinoline derivatives

A mixture of aromatic aldehyde (1 mmol), dimedone (1 mmol, 0.140 g) and 6-amino-1,3-dimethyluracil (1 mmol, 0.155 g) in the presence of the nano catalyst $Ag@SiO_2@SO_3H$ (0.003 g) was stirred at 80 °C for 10–40 minutes. After completion of the reaction according to the TLC test, warm absolute ethanol was added to the reaction mixture and stirred to extract the remaining starting materials and product. The catalyst was centrifuged and separated from the reaction mixture. The main product was purified by recrystallization in aqueous ethanol (90%).

Compound (1). IR (KBr, cm^{-1}): 3364, 3202 (N–H), 3029 (C–H–Ar), 2959 (C–H), 2879 (C–H), 1701 (C=O), 1656 (C=O), 1590 (C=N), 1506 (C=C), 1363 (C–N), 1256 (C–N), 1148 (C–N), 748 (C–H), 585 (C–H); ^{1}H NMR (250 MHz, DMSO-d_6): δ (ppm) 1.03 (s, 3H, CH_3), 1.11 (s, 3H, CH_3), 2.28–2.48 (m, 4H, CH_2), 3.09 (s, 3H, N–CH_3), 3.35 (s, 3H, N–CH_3), 5.47 (s, H, CH), 7.10 (s, 1H, Ar–H), 7.18–7.26 (m, 4H, Ar–H), 12.78 (s, 1H, NH); ^{13}C NMR (62.5 MHz, DMSO-d_6): δ (ppm) 27.5, 28.4, 29.2, 30.7, 31.5, 33.4, 44.0, 49.9, 88.3, 114.2, 125.6, 126.7, 128.3, 140.2, 150.6, 155.0, 164.1, 176.4, 199.8.

Compound (2). IR (KBr, cm^{-1}): 3225 (N–H), 3096 (C–H–Ar), 2965 (C–H), 2891 (C–H), 1703 (C=O), 1665 (C=O), 1640 (C=O), 1493 (C=C), 1381 (C–N), 1248 (C–F), 1209 (C–N), 766 (C–H), 503 (C–H); ^{1}H NMR (250 MHz, DMSO-d_6): δ (ppm) 0.85 (s, 3H, CH_3), 1.02 (s, 3H, CH_3), 1.96 (d, J = 15.75 Hz, 1H), 2.18 (d, J = 15.75 Hz, 1H), 2.51 (d, J = 12.25 Hz, 2H), 3.04 (s, 3H, N–CH_3), 3.43 (s, 3H, N–CH_3), 5.01 (s, H, CH), 6.93–7.07 (m, 3H, Ar–H), 7.25 (s, 1H,

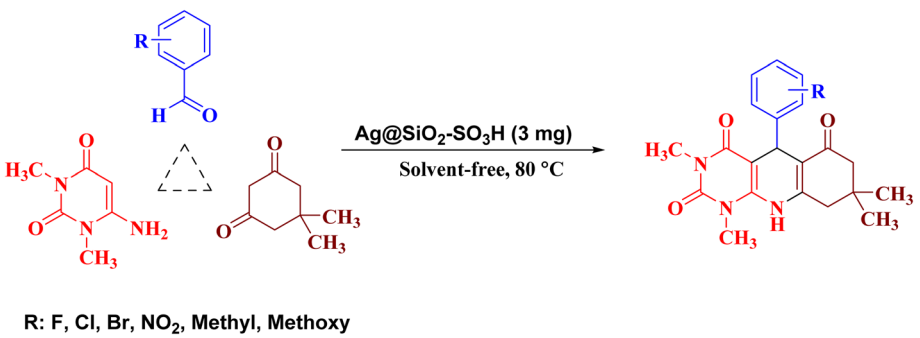

Scheme 1 Preparation of pyrimido[4,5-*b*]quinolines.

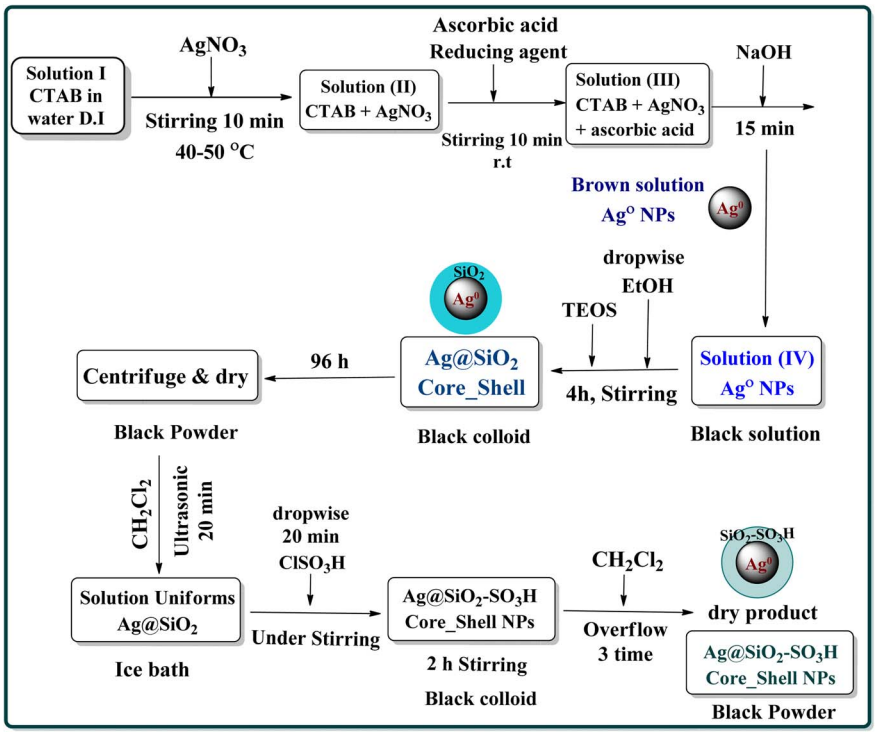

Fig. 1 Preparation of Ag@SiO_2–SO_3H.

Ar–H), 8.98 (s, 1H, NH); ^{13}C NMR (62.5 MHz, DMSO-d_6): δ (ppm) 26.6, 27.9, 29.5, 30.0, 30.6, 32.4, 50.4, 89.6, 110.9, 115.1, 115.5, 123.6, 128.1, 131.5, 133.6, 144.4, 150.3, 150.9, 158.4, 160.9, 162.3, 194.7.

Compound (3). IR (KBr, cm^{-1}): 3224 (N–H), 3095 (C–H–Ar), 2961 (C–H), 2872 (C–H), 1702 (C=O), 1664 (C=O), 1641 (C=O), 1496 (C=C), 1379 (C–N), 1244 (C–N), 1050 (C–Cl), 753 (C–H), 507 (C–H); ^{1}H NMR (250 MHz, DMSO-d_6): δ (ppm) 0.86 (s, 3H, CH_3), 1.01 (s, 3H, CH_3), 1.94 (d, J = 16.00 Hz, 1H), 2.17 (d, J = 16.00 Hz, 1H), 2.50 (d, J = 11.00 Hz, 2H), 3.02 (s, 3H, N–CH_3), 3.43 (s, 3H, N–CH_3), 5.14 (s, H, CH), 7.05–7.20 (m, 3H, Ar–H), 7.31 (d, J = 7.25 Hz, 1H, Ar–H), 8.97 (s, 1H, NH); ^{13}C NMR (62.5 MHz, DMSO-d_6): δ (ppm) 26.7, 27.9, 29.5, 30.6, 32.3, 34.1, 50.5, 89.9, 111.2, 126.7, 127.7, 129.5, 132.4, 133.0, 143.8, 144.6, 150.2, 150.9, 160.9, 194.7.

Compound (4). IR (KBr, cm^{-1}): 3225 (NH), 3095 (C–H–Ar), 2958 (C–H), 2871 (C–H), 1702 (C=O), 1663(C=O), 1641 (C=O), 1607 (C=O), 1492 (C=C), 1379 (C–N), 1150 (C–N),1080 (C–Br),

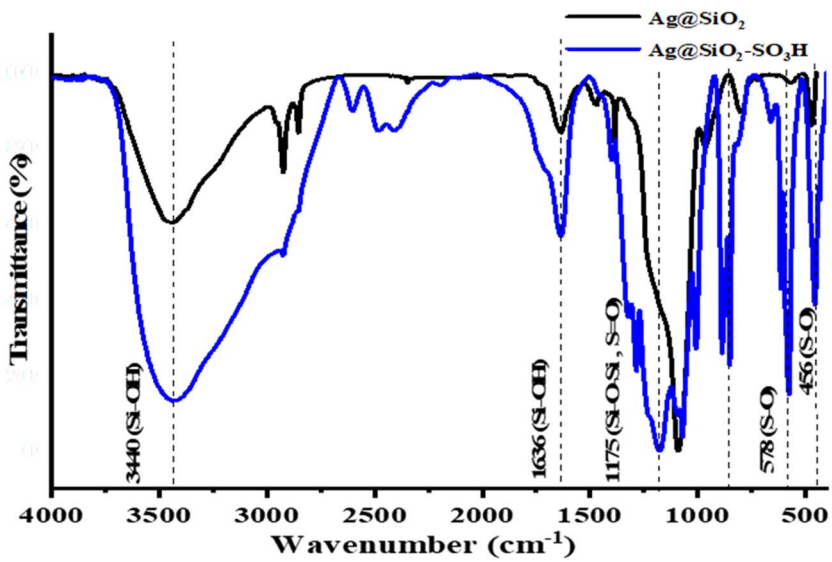

Fig. 2 FT-IR spectra of Ag@SiO_2–SO_3H and Ag@SiO_2 nanoparticles.

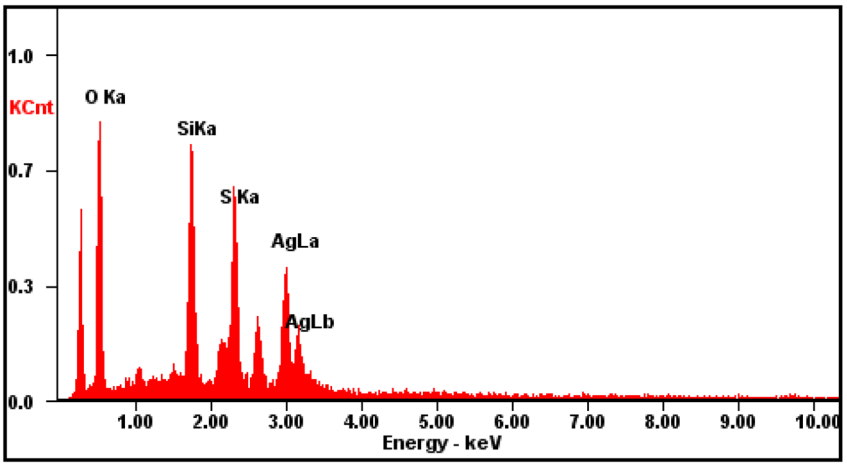

Fig. 3 EDX analysis of Ag@SiO_2–SO_3H.

751 (C–H), 508 (C–H); ^{1}H NMR (250 MHz, DMSO-d_6): δ (ppm) 0.87 (s, 3H, CH_3), 1.01 (s, 3H, CH_3), 1.94 (d, J = 16.50 Hz, 1H), 2.17 (d, J = 16.75 Hz, 1H), 2.51 (d, J = 12.00 Hz, 2H), 3.03 (s, 3H, N–CH_3), 3.44 (s, 3H, N–CH_3), 5.13 (s, H, CH), 6.96 (s, 1H, Ar–H), 7.18 (s, 1H, Ar–H), 7.28–7.38 (m, 2H, Ar–H), 8.94 (s, 1H, NH); ^{13}C NMR (62.5 MHz, DMSO-d_6): δ (ppm) 26.9, 27.9, 29.4, 30.6, 32.3, 36.2, 50.5, 90.3, 111.6, 123.5, 127.4, 127.9,132.4, 132.8, 144.5, 145.6, 150.1, 150.9, 194.7.

Compound (5). IR (KBr, cm^{-1}): 3210 (NH), 3083 (C–H–Ar), 2954 (C–H), 2832 (C–H), 1702 (C=O), 1665 (C=O), 1641 (C=O), 1501 (C=C), 1380 (C–N), 1221 (C–N), 1046 (C–O), 805 (C–H), 507 (C–H); ^{1}H NMR (250 MHz, DMSO-d_6): δ (ppm) 0.82 (s, 3H, CH_3), 1.01 (s, 3H, CH_3), 1.92 (d, J = 15.75 Hz, 1H), 2.15 (d, J = 16.00 Hz, 1H), 2.48 (s, 2H), 3.03 (s, 3H, N–CH_3), 3.33 (s, 3H, N–CH_3), 3.61 (s, 3H, O–CH_3), 3.64 (s, 3H, O–CH_3), 4.85 (s, H, CH), 6.62 (s, 1H, Ar–H), 6.72–6.75 (m, 2H, Ar–H), 8.92 (s, 1H, NH); ^{13}C NMR (62.5 MHz, DMSO-d_6): δ (ppm) 18.9, 26.3, 27.9, 29.7, 30.4, 32.3, 33.3, 50.6, 55.5, 56.2, 89.2, 110.2, 111.3, 112.5, 118.5, 134.4, 144.7, 150.4, 151.0, 152.7, 153.8, 160.9, 194.7.

Results and discussions

For the preparation of sulfonic acid supported on silica shell silver nanoparticles, Ag^0 nanoparticles were initially prepared from Ag^+. For this purpose, cetyltrimethylammonium bromide (CTAB) was dissolved in deionized water under stirring at 40–

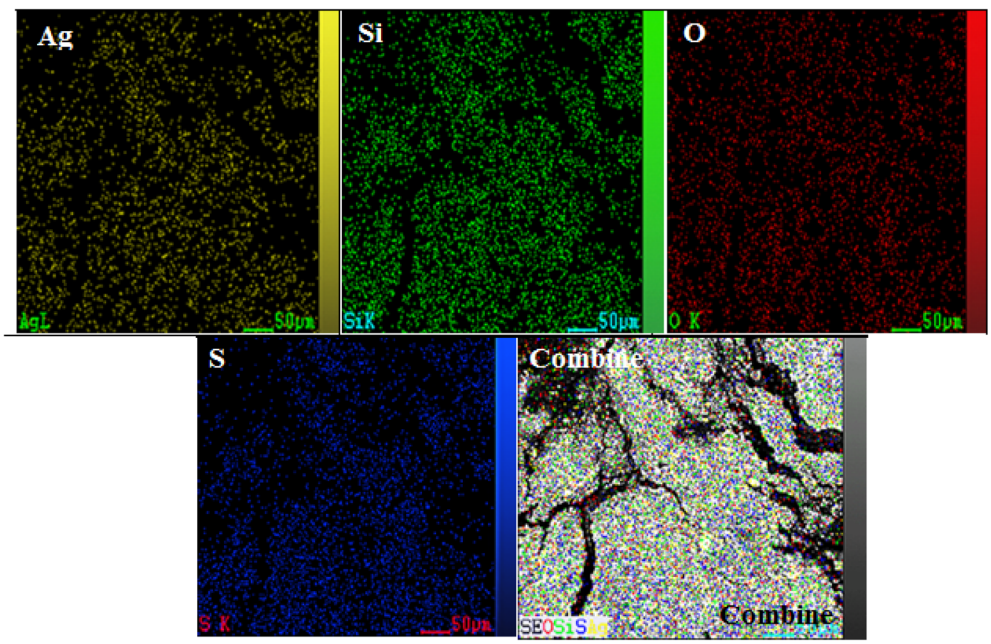

Fig. 4 SEM-coupled EDX (SEM mapping) of Ag@SiO_2–SO_3H.

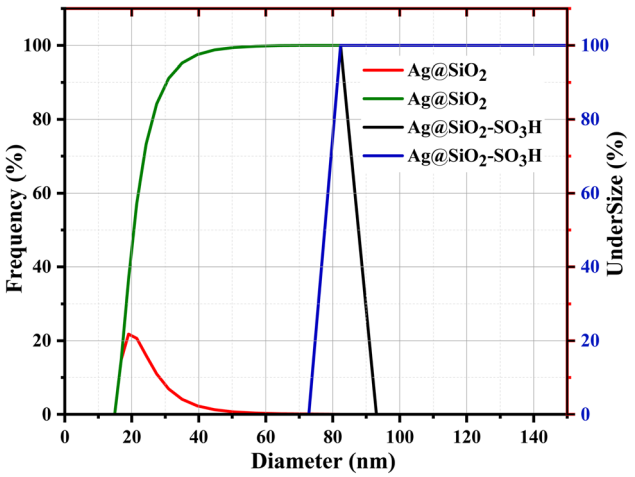

Fig. 5 Comparison of DLS of $Ag@SiO_2$ and $Ag@SiO_2$–SO_3H.

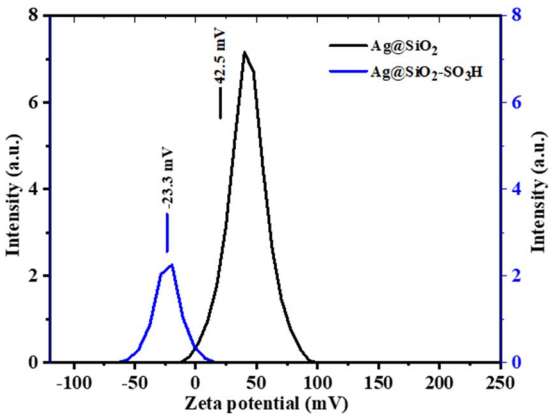

Fig. 6 Comparison of the zeta potentials of $Ag@SiO_2$ and $Ag@SiO_2$–SO_3H.

50 °C, then silver nitrate and ascorbic acid were added under stirring to this reaction solution, during which the color of the solution darkened. To coat the Ag^0 nanoparticles with silica, solid sodium hydroxide was added under stirring, then tetraethyl orthosilicate (TEOS) and ethanol (5 mL) were added dropwise during three hours under stirring at room temperature to give silica-coated silver nanoparticles ($Ag@SiO_2$) after 96 hours. In the last step, $Ag@SiO_2$ as a support was functionalized with sulfonic acid *via* reaction with chlorosulfonic acid to give $Ag@SiO_2$–SO_3H as the final catalyst (Fig. 1).

The preparation of the $Ag@SiO_2$–SO_3H was confirmed by various analyses such as Fourier transform infrared spectroscopy (FT-IR), dynamic light scattering (DLS), zeta potential (ZP), atomic force microscopy (AFM), field emission-scanning electron microscopy (FE-SEM), energy dispersive X-ray (EDX), SEM coupled EDX (SEM mapping), transmission electron microscopy (TEM), X-ray diffraction (XRD) analysis, X-ray photoelectron spectroscopy (XPS), Brunauer–Emmett–Teller analysis (BET), and thermogravimetric analysis (TGA).

FT-IR spectroscopy was performed to identify specific functional groups in the structure of the catalyst. In the FT-IR spectrum of $Ag@SiO_2$, the characteristic absorption peak at 460 cm^{-1} corresponding to the Si–O bending vibration was observed.[72] The identified absorption peaks at 1039, 1261 and 1384 cm^{-1} correspond to Si–O–Si bending vibrations, and symmetric and asymmetric Si–O–Si stretching vibrations, respectively. Absorption peaks at 1634 and 3419 cm^{-1} correspond to hydroxyl groups in Si–OH, OH bending and stretching vibrations, respectively.[72] The presence of a Si–O functional group in the FT-IR spectrum indicates the successful formation of $Ag@SiO_2$ nanoparticles (Fig. 2). In the FT-IR spectrum of $Ag@SiO_2$–SO_3H, characteristic absorption peaks at 887 and 1007 cm^{-1} correspond to S–O bending and stretching vibrations, 1070 and 1175 cm^{-1} correspond to S=O symmetric and asymmetric bending, respectively, and 1296 cm^{-1} corresponds to S=O stretching vibrations. The presence of S–O bonds is evidence for the successful formation of the catalyst (Fig. 2).

The energy dispersive X-ray (EDX) spectrum of $Ag@SiO_2$–SO_3H nanoparticles is presented in Fig. 3. This pattern clearly indicates the presence of expected elements, namely, silver, silicon, sulfur and oxygen, in the structure of the core–shell catalyst nanoparticles. The extra peaks observed in this spectrum are caused by gold and platinum impurities introduced during the coating for analysis. Thus, the EDX analysis confirms the successful formation of $Ag@SiO_2$–SO_3H (Fig. 3).

To determine the distribution of elements in $Ag@SiO_2$–SO_3H, SEM-coupled EDX (SEM mapping) analysis was performed. Based on this analysis, it was found that elements including silver, oxygen, silicon and sulfur were well dispersed over the structure of $Ag@SiO_2$–SO_3H with an appropriate distribution (Fig. 4).

To determine the size and distribution of the catalyst, dynamic light scattering (DLS) analysis was performed. The average particle sizes of $Ag@SiO_2$ and $Ag@SiO_2$–SO_3H were observed to be 22.6 and 77.5 nm, respectively. In DLS analysis, a uniform sample of nanoparticles is shown as a narrow peak at a specific size; on the other hand, a broad peak or multiple peaks can be related to a less uniform sample of nanoparticles with a range of particle sizes. The observed sharp and narrow peak for $Ag@SiO_2$–SO_3H nanoparticles in the DLS analysis confirms the uniformity of the sample. The functionalization of the $Ag@SiO_2$ nanoparticles with SO_3H increased the size and acidity of the prepared nanoparticles (Fig. 5).

Table 1 Comparison of DLS, ZP and pH of the $Ag@SiO_2$ and $A@SiO_2$–SO_3H

Sample	DLS (nm)	ZP (mv)	pH
$Ag@SiO_2$	22.6	42.5	3.7
$Ag@SiO_2$–SO_3H	77.5	−23.3	2.3

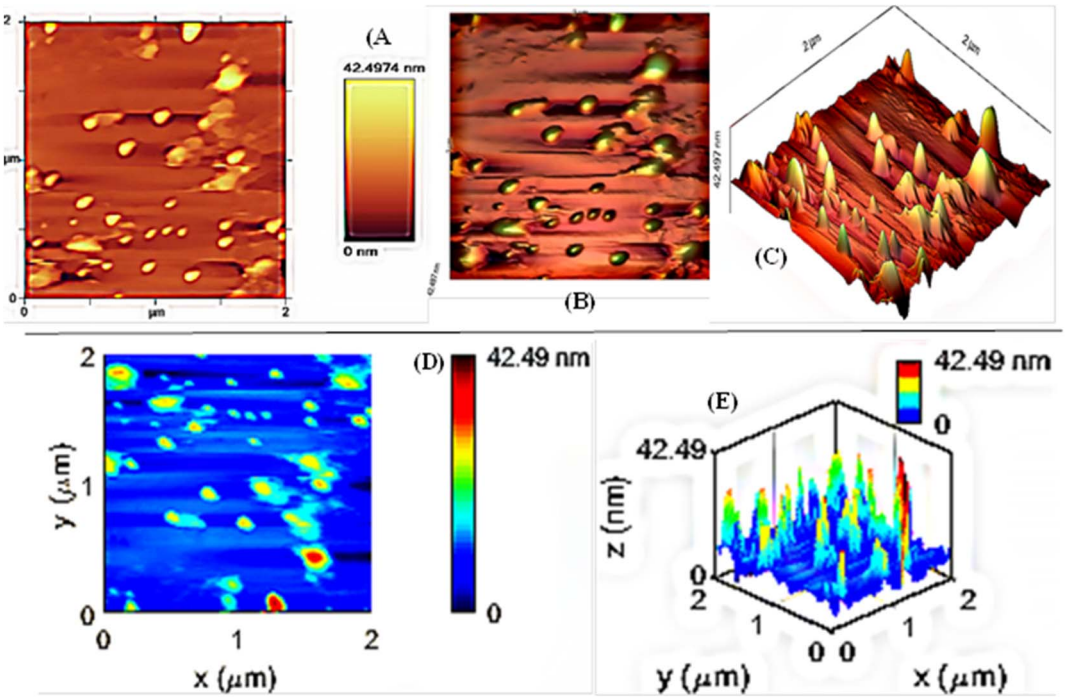

Fig. 7 AFM topography images of Ag@SiO_2–SO_3H in dimensions of 2 × 2 microns. (A) initial image, (B) 2D image, (C) 3D image, (D) improved 2D image in Mat lab with color bar, (E) improved 3D image in Mat lab with color bar.

To determine the stability of Ag@SiO_2 and Ag@SiO_2–SO_3H nanoparticles, their zeta potentials were measured. The zeta potentials were 42.5 and −23.3 mV, respectively (Fig. 6). According to the standards of the DLS method, the particle size and zeta potential values indicate the stability of the catalyst (Table 1). The negative zeta potential indicates a high repulsion

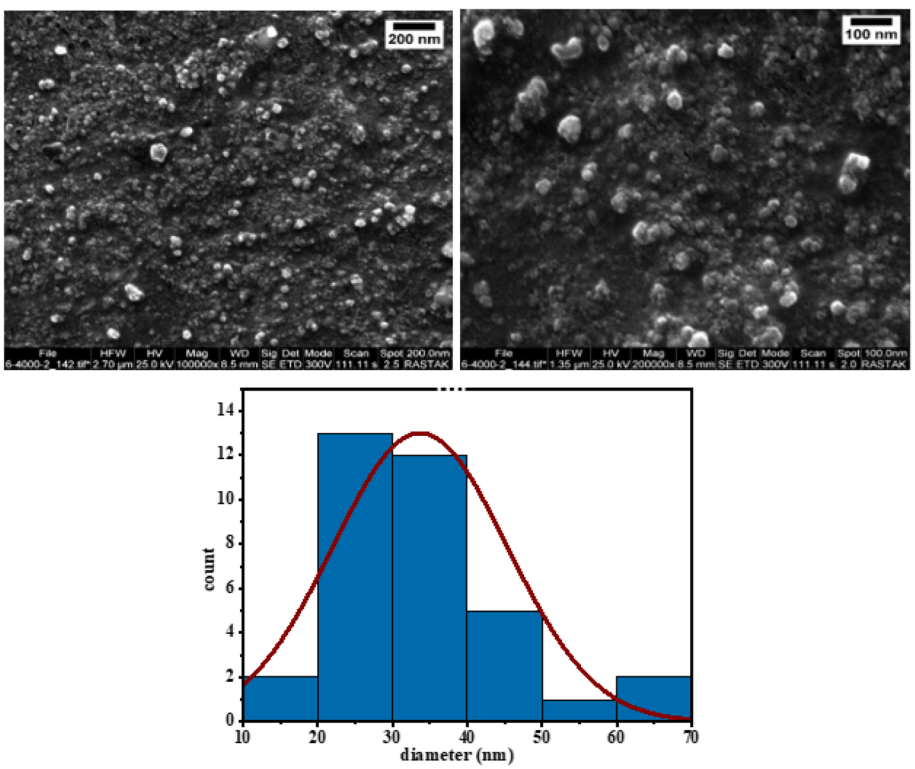

Fig. 8 FE-SEM images (micrographs) of the Ag@SiO_2–SO_3H.

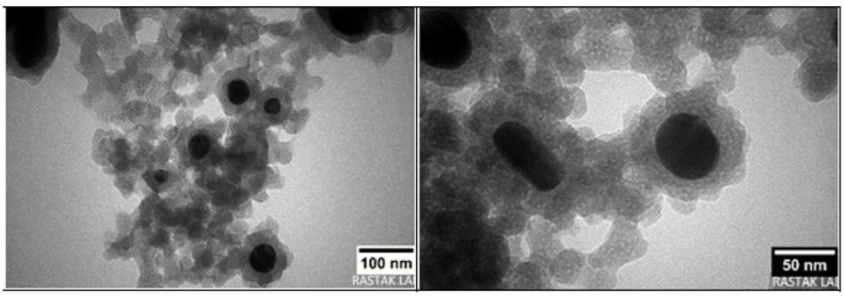

Fig. 9 TEM images of the Ag@SiO_2–SO_3H sample.

between nanoparticles; this repulsive force prevents aggregation and increases the long-term stability of metal colloids.[73]

The boundary between unstable and stable suspensions is often found at 30 or −30 mV; *i.e.*, particles with zeta potentials that are more positive than 30 mV or more negative than −30 mV. If a zeta potential is more positive than 30 mV and more negative than −30 mV, the resulting suspension is stable. A zeta potential with values more positive than −15 mV indicates that the suspension is on the verge of agglomeration.[74] The coagulation or flocculation process occurs more rapidly when the zeta potential is in the range of 30 mV. The observed zeta potential thus reflects the stability of the particles.

To study the Ag@SiO_2–SO_3H nanoparticles in more detail, atomic force microscopy (AFM) images were recorded. The 2D and 3D topographies of the synthesized Ag@SiO_2–SO_3H are shown in Fig. 7. The initial image with a color bar is shown in Fig. 7A. Fig. 7B and D show 2D and enhanced images (improved with MATLAB software) that reveal large numbers of small spherical particles. The distribution of the particles is uniform and the size of the particles in this image is 42.5 nm. In the 3D image (Fig. 7C), the distribution of particles is uniform, and the image shape is improved with MATLAB software. The color change in the color bar from light to dark indicates an increase in size. The topography of the AFM images reveals that Ag@SiO_2–SO_3H was prepared with a high number of particles of small sizes. The surfaces show very low roughness with a homogeneous structure (Fig. 7).

Field emission-scanning electron microscopy (FE-SEM) was used to determine the size and morphology of the catalyst particles (Fig. 8). The micrographs show that the particles were prepared on the nanometer scale, typically less than 100 nm. The spherical nanoparticles that are observed in the images are related to the Ag@SiO_2–SO_3H nanoparticles. The distribution of particles is depicted as a histogram in Fig. 8.

Transmission electron microscopy (TEM) of Ag@SiO_2–SO_3H was conducted to observe the size and core–shell structure of Ag@SiO_2–SO_3H nanoparticles. The TEM images confirmed that the Ag@SiO_2–SO_3H nanoparticles have a core–shell structure. These nanoparticles have a dark core of Ag and light shell of sulfonic–silica, indicating that Ag nanoparticles are coated with silica and functionalized with sulfonic acid (Fig. 9).

The X-ray diffraction (XRD) pattern of Ag@SiO_2–SO_3H contained peaks at 2θ = 27.59, 31.97, 38.11, 44.30, 45.86, 54.37, 57.00, 64.44, 76.08, 77.40 and 81.54°; for silver, this corresponds to miller indices (*hkl*) at (111), (002), (022), (113) and (222) crystal planes, respectively, as previously reported for Ag@SiO_2 nanoparticles.[75] The crystal sizes of the prepared catalyst particles were calculated based on Debbie Scherer's equation and found to be 33.67, 30.75, 20.58, 11.79, 24.57, 23.67, 20.66, 5.68, 9.31, 3.97 and 2.31 nm (Fig. 10).

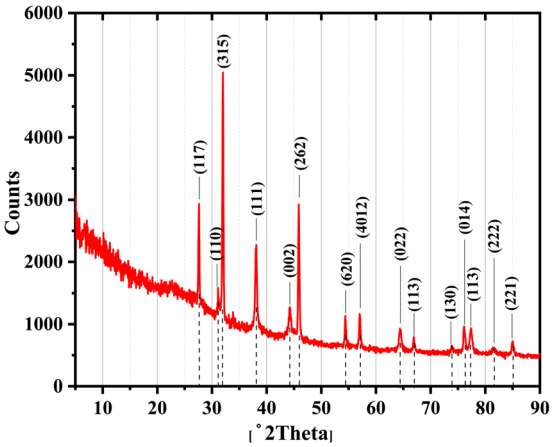

Fig. 10 XRD pattern of the Ag@SiO_2–SO_3H.

X-ray photoelectron spectroscopy (XPS) was conducted for the AgNPs and the binding energies of electrons observed in the XPS spectrum were compared to the reported values. The reference peak for carbon is 284.5 eV according to the references. On the other hand, the reference peak in the sample spectrum was observed at 289.2 eV; to correct for this difference, the binding energy of the observed peaks should be reduced by 4.7 eV (289.2 − 284.5 = 4.7 eV).[76] The survey spectrum shows what elements are present in the sample (the carbon peak is considered as a reference peak), and the displacement of other elements relative to carbon is measured. In the survey spectrum, carbon, silver and oxygen elements are observed. The presence of silver is evidence of the synthesis of the nanoparticles whereas the presence of carbon and oxygen can be due to surface contamination introduced during sample preparation or from oxygen in the air (or due to the materials used for synthesis, such as CTAB or ascorbic acid).[77] Two peaks, $3d_{5/2}$ and $3d_{3/2}$, with binding energies of 372.7 eV and 378.9 eV, (372.7

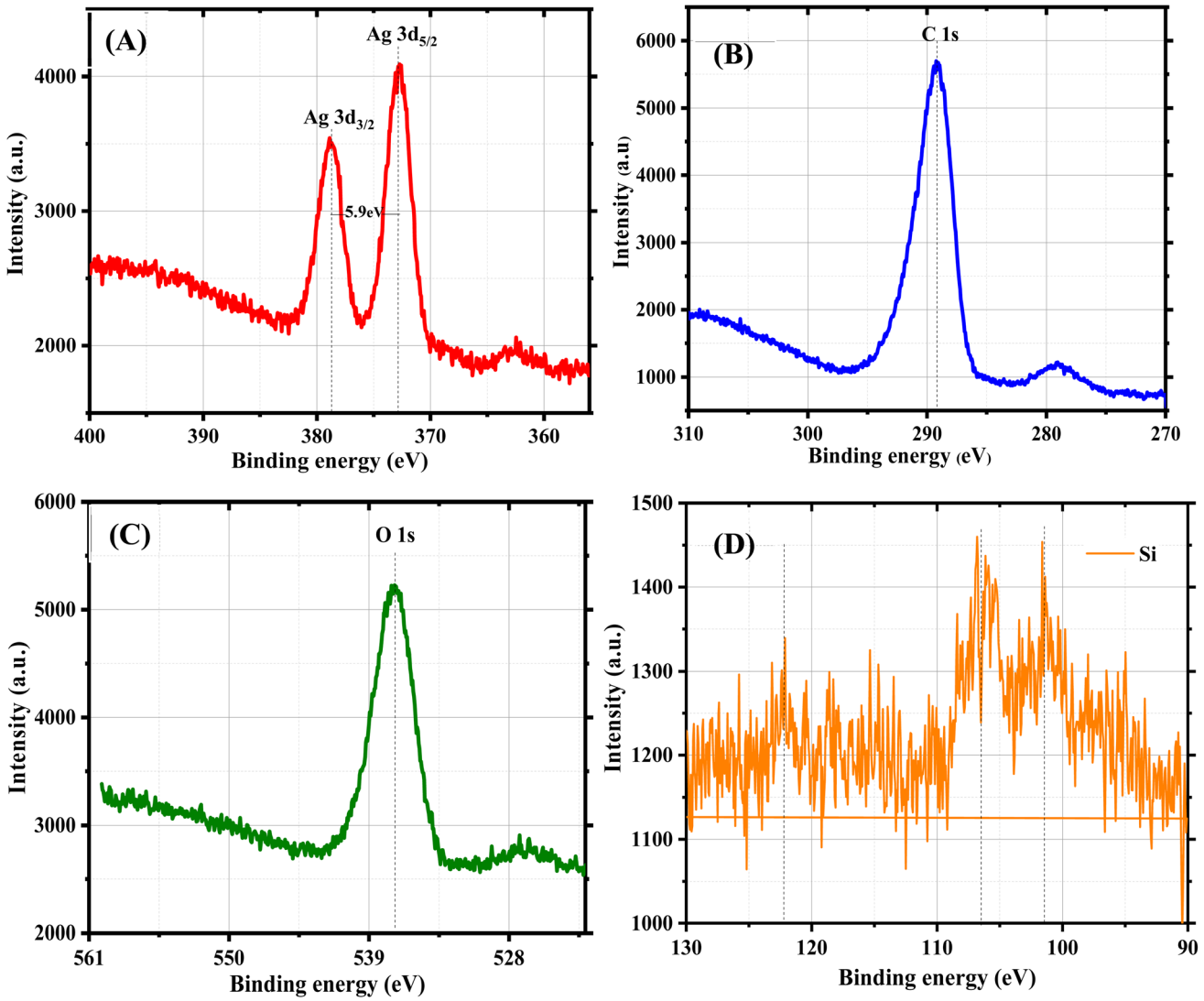

Fig. 11 High-resoluotion XPS spectra: (A) 3d Ag, (B) 1s C, (C) 1s O, (D) Si.

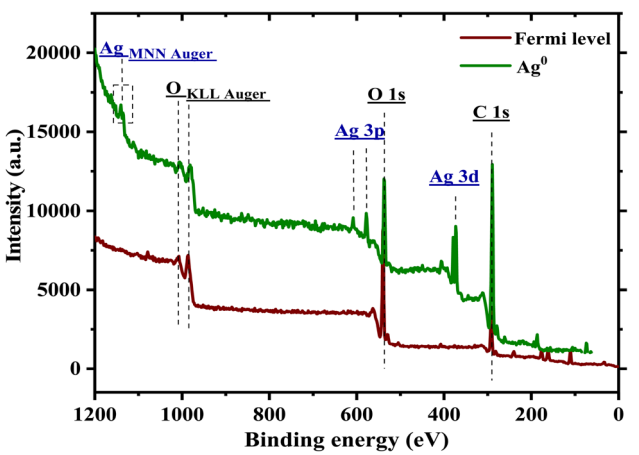

Fig. 12 XPS survey scan (spectra) of the AgNPs and valence band spectra in the vicinity of the Fermi level.

Table 2 XPS of AgNPs

	Binding energy (eV)	
Peaks	Reported	(Lit)[71]
Ag Auger	1136.0	1134.9
Ag $3p^1$	603.19	604.0
Ag $3p^3$	573.3	573.6
Ag 3d	368.47–374.45	368.4
C 1s	285.0	284.5

− 4.7 = 368 eV and 378.9 − 4.7 = 373.9 eV) are attributed to the presence of Ag^0.[76] The difference in energy between the two silver peaks is ΔBE = 5.98 eV.[76] For the oxygen element, the binding energy is 537 eV (537 − 4.7 = 532.3 eV), the binding energy of 578 eV corresponds to silver 3p3 and 608 eV corresponds to the silver 3p1 layer (608 − 4.7 = 603.3 and 578 − 4.7 = 573.3 eV).[76] Two broad peaks with binding energy 1007.15–981.7 eV (1007.15 − 4.7 = 1002.45 eV and 981.7 − 4.7 = 977 eV)

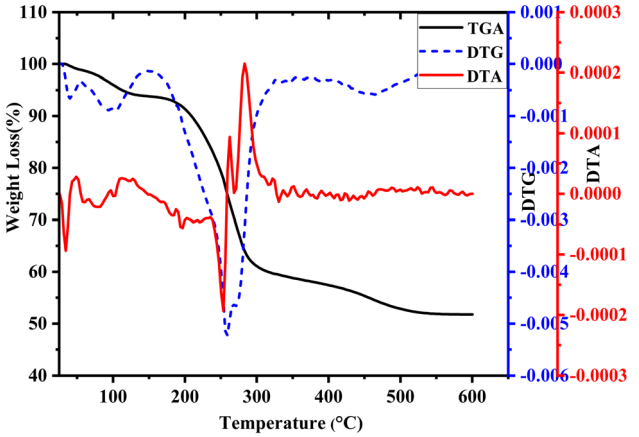

Fig. 13 TGA, DTG and DTA of Ag@SiO_2–SO_3H.

correspond to oxygen electrons and the broad peak 1140.2 eV (1140.2 − 4.7 = 1135.5 eV) is related to silver Auger electrons (Fig. 11, 12 and Table 2).[76]

Table 3 BET analysis of the Ag@SiO_2–SO_3H

Ag@SiO_2–SO_3H			
a_{SBET} (m^2 g^{-1})	BET (C) nm	Total pore (cm^3 g^{-1})	Mean pore diameter (nm)
1.91	357.24	0.024	50.24

The thermal stability of the catalyst was investigated by thermal gravimetric analysis (TGA), derivative thermogravimetric (DTG) analysis and differential thermal analysis (DTA). According to the results obtained from this analysis, Ag@SiO_2–SO_3H can be used from room temperature up to 190 °C, with only 5.1% weight loss in this temperature range (Fig. 13). In this study, two-step weight losses were observed in the TG diagram of the catalyst. The first weight loss step is attributed to the loss of physically adsorbed solvents on the surface of the catalyst and the second weight loss occurred upon the loss of SO_3H

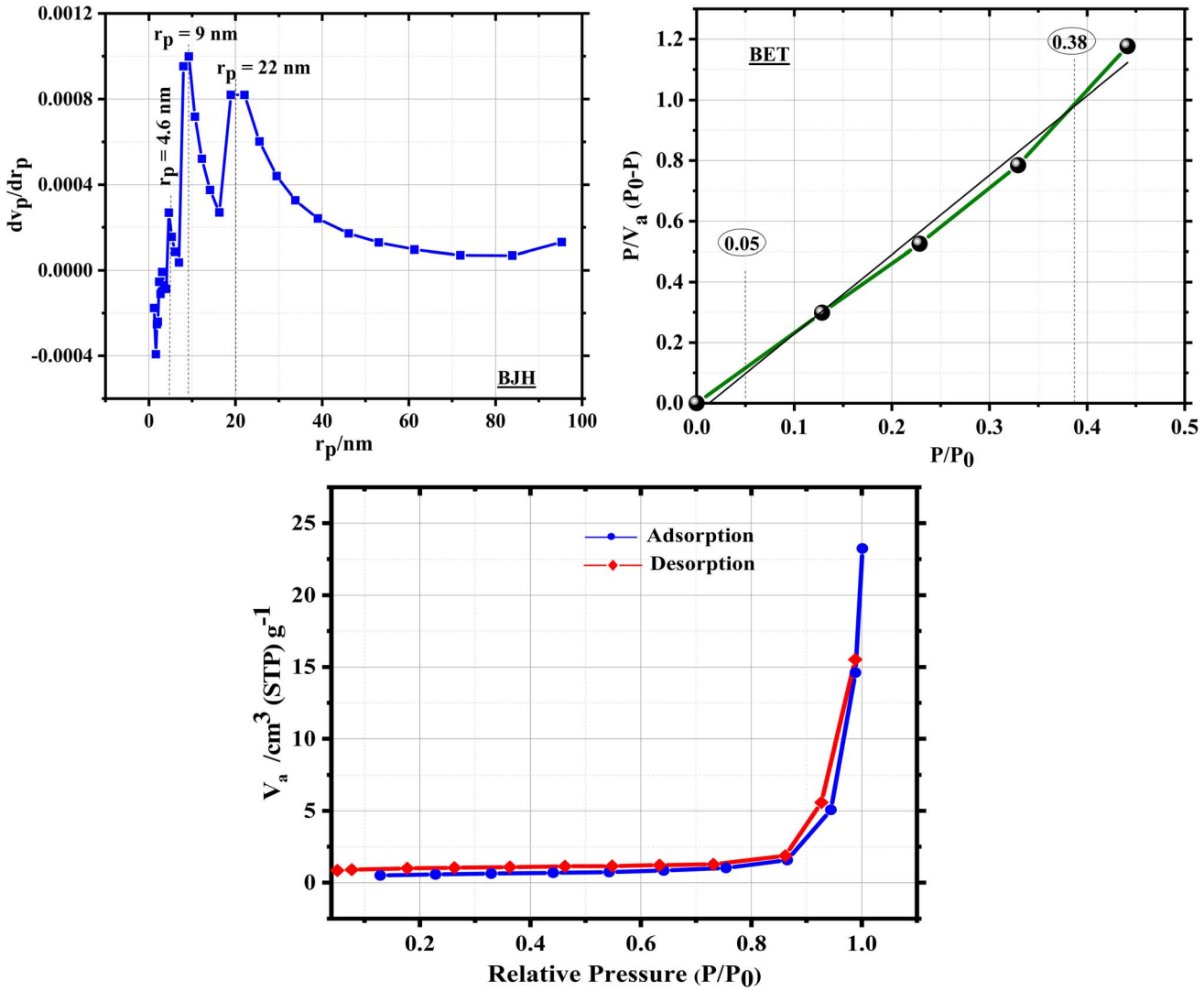

Fig. 14 BJH, BET and adsorption and desorption isotherms for the Ag@SiO_2–SO_3H.

Table 4 Optimization of the reaction conditions for the model reaction

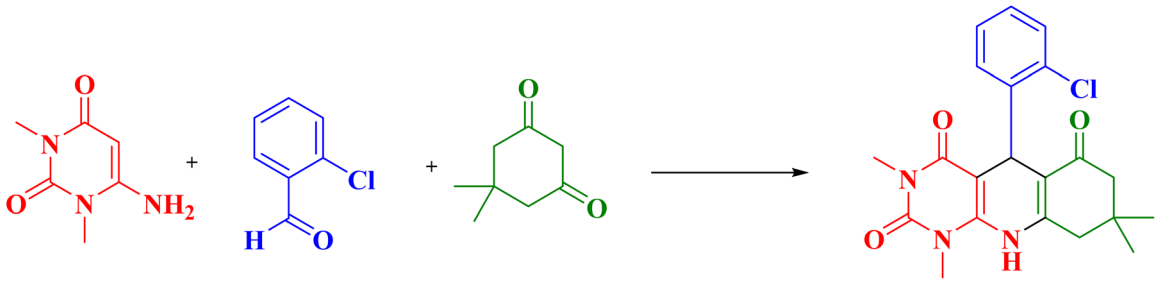

Entry	Solvent	Catalyst amount (mg)	Temp. (°C)	Time (min)	Yield[a] (%)
1	—	—	80	120	10
2	—	1.5	80	50	47
3	—	3	80	10	95
4	—	4.5	80	10	52
5	Ethanol	3	Reflux	10	66
6	CH_3Cl	3	Reflux	10	88
7	Ethyl acetate	3	Reflux	10	74
8	DCM	3	Reflux	10	72
9	DMF	3	Reflux	10	74
10	*n*-Hexane	3	Reflux	10	52
11	—	3	50	30	49
12	—	3	110	10	70

[a] Isolated yield.

groups from the catalyst above 190 °C.[78] Above this temperature, the Ag@SiO_2 core–shell structure was maintained with high thermal stability.[79,80] According to the TGA, DTG and DTA analyses, it is concluded that this catalyst shows acceptable thermal stability in chemical reactions.[78–80]

According to IUPAC classification, the hysteresis loop in the adsorption and desorption curve is of type H4, which is related to mesoporous materials, and the adsorption and desorption profiles do not match, which is caused by factors such as the shape of the cavities, the structure of the material, the method of producing the material, and the physical purity of the material. According to IUPAC, the morphology of particles with irregular internal cavities is in the form of narrow slits, which shows a mixture of non-uniform mesopores and micropores. In materials that exhibit this type of hysteresis loop, the adsorbate–adsorbate interactions are relatively strong (Fig. 14). Based on the profile of the BJH diagram (Fig. 14), the maximum size of the holes was observed in the range of 2 to 22 nm (with a peak at 9 nm), which corresponds to the diameter of the holes obtained from BET and shows the catalytic activity of the catalyst for the synthesis of acyclic reactions. The specific surface area was 1.91 ($m^2\ g^{-1}$), the BET constant value was 357.24 nm, the total pore volume was 0.024 ($cm^3\ g^{-1}$), and the average pore diameter was 50 nm. For the BET diagram, deviation from the straight line occurred at approximately 0.33 and the interpretable range in BET was 0.05–0.3 (Fig. 14 and Table 3).

After the preparation and identification of Ag@SiO_2–SO_3H, its catalytic ability was tested with the condensation reaction of 2-chlorobenzaldehyde with dimedone and 6-amino-1,3-dimethyluracil to establish the best reaction conditions. Temperature, catalyst amounts and various solvents, including ethanol, chloroform, dichloromethane, ethyl acetate and dimethylformamide, were investigated; solvent-free conditions were also examined. It was found that acceptable results were obtained when the model reaction was carried out in the presence of 3 mg of catalyst under solvent-free conditions (Table 4).

With the optimized reaction conditions in hand, the generality of the method was studied with a series of aromatic aldehydes containing electron-donating or electron-withdrawing groups and halogen on their ring to prepare the corresponding pyrimido[4,5-*b*]quinoline derivatives (Table 5). All the products were prepared in high yields and short reaction times.

A suggested mechanism, supported by previous reports,[16,18,35,81] illustrates the role of the catalyst in the preparation of pyrimido[4,5-*b*]quinolines (Scheme 2). The enol form of dimedone first reacts with the aldehyde, which is activated with Ag@SiO_2–SO_3H to prepare (I). By the elimination of one molecule of H_2O, intermediate (II) is generated as a Michael acceptor. In the next step, 6-amino-1,3-dimethyluracil reacts with the presented Michael acceptor (II) to prepare (III) after tautomerization. Finally, intramolecular nucleophilic attack of the amine on the carbonyl group in intermediate (III) and ring

Table 5 Synthesis of pyrimido[4,5-*b*]quinoline derivatives in the presence of the catalyst

Entry	Product	Time (min)	Yield[a] (%)	M.p. °C (Lit.)
1	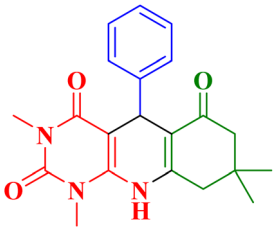	15	89	244–245 (253–255)[17]
2	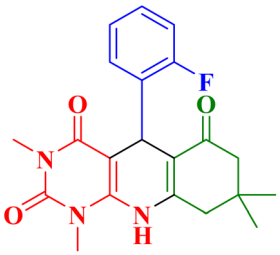	10	81	346–350 (—)
3	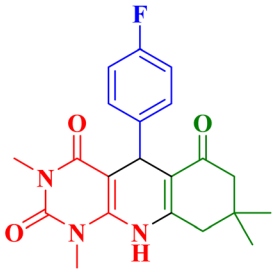	12	89	247–249 (238–240)[37]
4	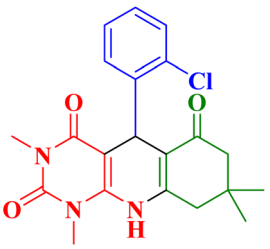	10	95	347–351 (350–355)[17]
5	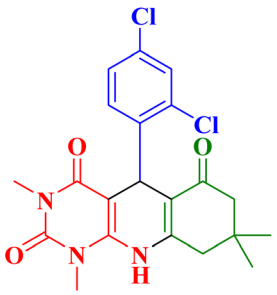	19	85	293–296 (>300)[24]

Table 5 (*Contd.*)

Entry	Product	Time (min)	Yield[a] (%)	M.p. °C (Lit.)
6	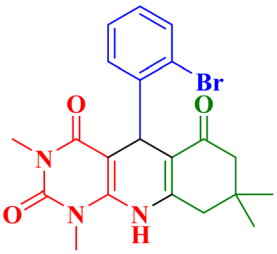	24	79	346–349 (—)
7	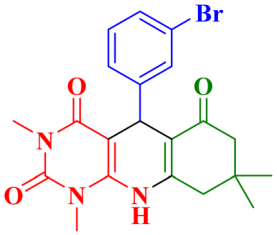	25	78	289–293 (285–287)[24]
8	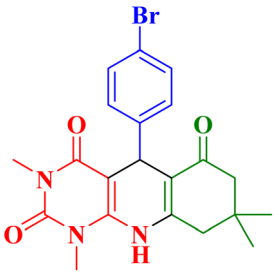	30	85	296–298 (>300)
9	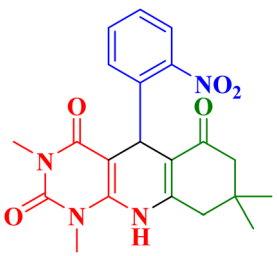	10	85	288–289 (292–294)[24]
10	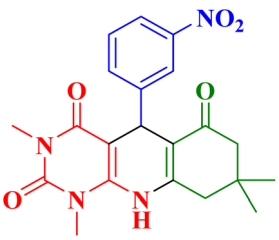	40	83	298–301 (300–303)[17]

Table 5 (*Contd.*)

Entry	Product	Time (min)	Yield[a] (%)	M.p. °C (Lit.)
11	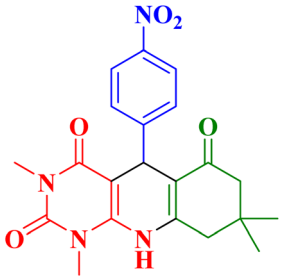	10	97	225–229 (226–229)[35]
12	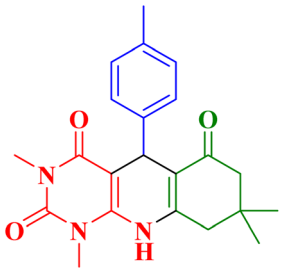	35	95	315–320 (>300)[24]
13	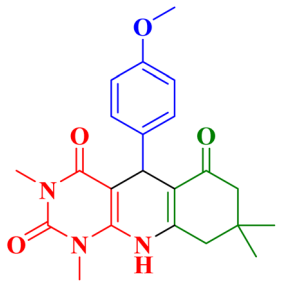	20	93	278–282 (301–303)[35]
14	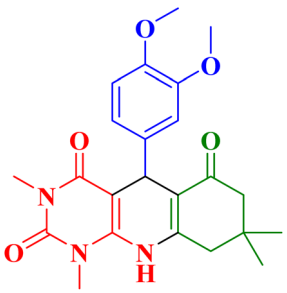	25	99	310–314 (>300)[32]
15	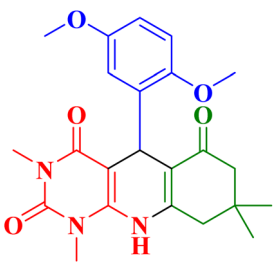	10	98	280–284 (208–212)[19]

[a] Isolated yield.

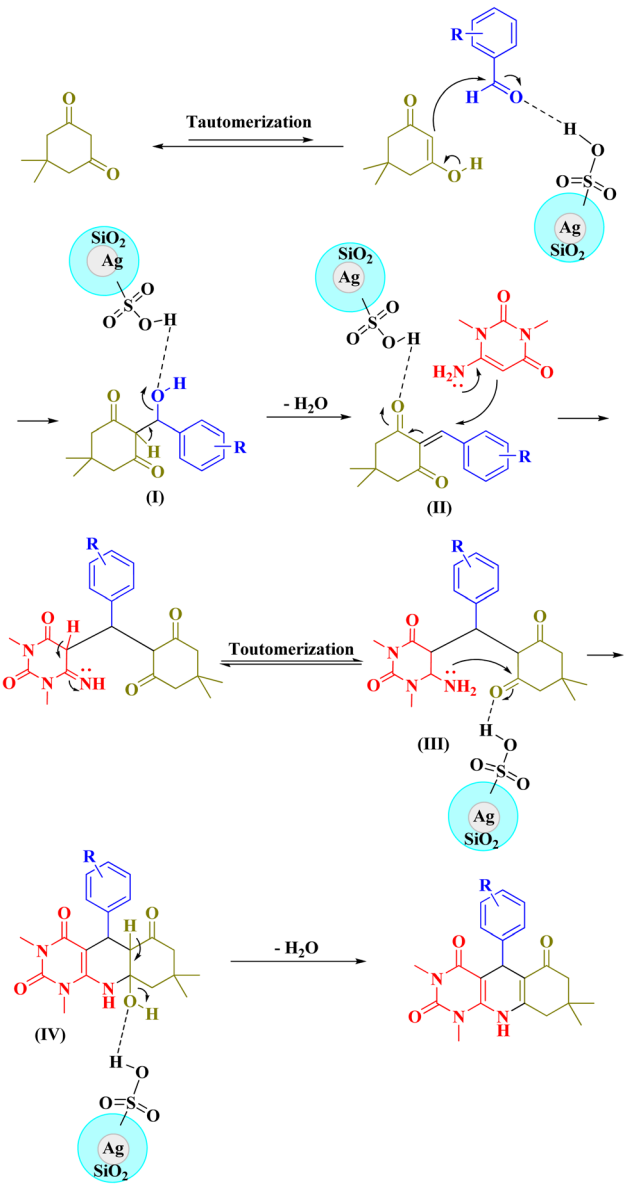

Scheme 2 . Proposed mechanism for the preparation of pyrimido[4,5-*b*]quinolines.

closure occur, followed by the removal of one molecule of H_2O, to generate the final product (Scheme 2).

In this study, silver nanoparticles were used as a suitable support for preparing an acidic catalyst with a nanoscale core–shell structure. Coating the silver nanoparticles with silica prevents the particles from coalescing and agglomerating, and also prevents these particles from undergoing reactions such as oxidation and reduction, and protects them from interacting with the acidic part of the catalyst. Coating the silver nanoparticles with silica increases the stability of the catalyst and its lifetime. The design of this solid acidic catalyst at the nanoscale using silver nanoparticles as a support increases its contact surface, accelerates the reaction rate, and simplifies the use of the catalyst.

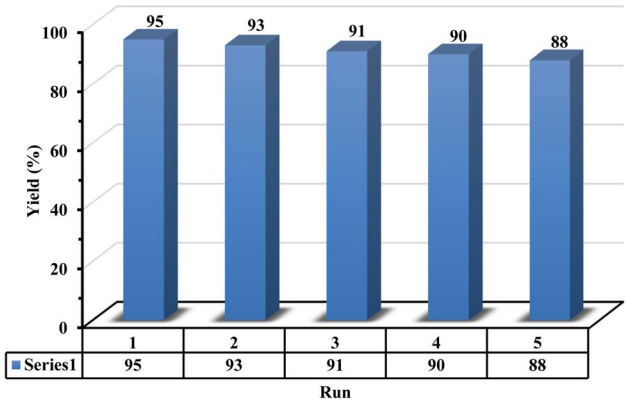

Fig. 15 Recovery of $Ag@SiO_2–SO_3H$.

To investigate the reusability of $Ag@SiO_2–SO_3H$, the reaction of 4-chlorobenzaldehyde with dimedone and 6-amino-1,3-dimethyluracil was carried out in the presence of this catalyst; upon completion of the reaction, warm absolute ethanol was added and the reaction mixture was stirred to extract the remaining starting materials and product. The catalyst was centrifuged and separated from the reaction mixture. The recovered catalyst was successfully reused in four further reactions and the related product was prepared with acceptable yield and suitable reaction time (Fig. 15). The reaction time for each reaction was 15 minutes. To confirm that the structure of the catalyst was unchanged after recovery, the FT-IR spectra of fresh and reused catalysts were compared (Fig. 16). According to this investigation, the important bond vibrations related to specific bonds were retained.

The preparation of the related pyrimido[4,5-*b*]quinoline by the reaction of 4-nitrobenzaldehyde with dimedone and 6-amino-1,3-dimethyluracil catalyzed by $Ag@SiO_2@SO_3H$ was compared in terms of yield and reaction time under a range of conditions and catalysts; the results are summarized in Table 6. The results indicate that the present catalyst and conditions delivered superior outcomes to those obtained using previously reported methods.

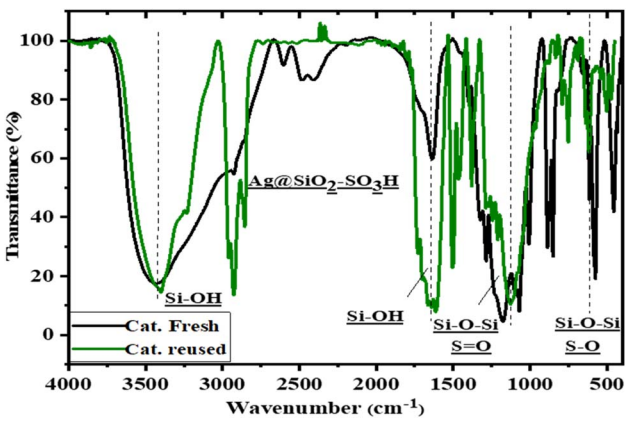

Fig. 16 FT-IR spectra of the fresh and reused $Ag@SiO_2–SO_3H$.

Table 6 Comparison of the present catalyst with other catalysts for the reaction of 4-nitrobenzaldehyde with dimedone and 6-amino-1,3-dimethyluracil

Entry	Catalyst (amount)	Condition	Time (min)	Yield[a] (%)	Ref.
1	$[H_2\text{-DABCO}][ClO_4]_2$ (0.19 mmol, 0.060 g)	H_2O, 75 °C	30	85	21
2	GO/Fe_3O_4@TRMS@BDSA@SO_3H (0.05 g)	SF, 70 °C	14	92	37
3	Nano-[Cu–$4C_3$NSP]$(Cl)_2$ (6 mol%)	EtOH, 60 °C	45	80	35
4	[Dsim]HSO_4, (0.25 mmol)	EtOH, 70 °C	15	92	81
5	TiO_2/PCN (0.006 g)	EtOH, reflux	40	80	38
6	Nano-[Fe_3O_4@SiO_2/*N*-propyl-1-(thiophene-2-yl)ethanimine][$ZnCl_2$] (0.02 g)	EtOH, 60 °C	20	94	18
7	$RuCl_3 \cdot xH_2O$ (3 mol%)	H_2O, 85 °C	25	91	39
8	TEBAC (0.15 g)	H_2O, 90 °C	13	86	40
9	Ag@SiO_2–SO_3H (10 mol%)	SF, 80 °C	10	97	Our work

[a] Isolated yield.

Conclusion

Sulfonic acid supported on silica-coated silver nanoparticles (Ag@SiO_2–SO_3H) were prepared by placing sulfonic acid on Ag@SiO_2 nanoparticles and the resulting material was studied using a series of analytical techniques. Ag@SiO_2–SO_3H was assessed as a novel heterogeneous acidic catalyst for the synthesis of pyrimido[4,5-*b*]quinolines and acceptable results were obtained for the reaction of dimedone and 6-amino-1,3-dimethyluracil with various aromatic aldehydes at 80 °C under solvent-free conditions.

Data availability

The datasets supporting this article have been uploaded as part of the ESI.†

Conflicts of interest

There are no conflicts to declare.

Acknowledgements

We thank the Hamedan University of Technology for financial support to our research group.

References

1 A. Drabczynska, C. E. Muller, A. Schiedel, B. Schumacher, J. K. Wojciechowska, A. Fruzinski, W. Zobnina, O. Yuzlenko and K. Kiec-Kononowicz, *Bioorg. Med. Chem.*, 2007, **15**, 6956–6974.
2 A. A. Joshi and C. L. Viswanathan, *Anti-Infect. Agents Med. Chem.*, 2006, **5**, 105–122.
3 J. A. Valderrama, P. Colonelli, D. Vasquez, M. F. Gonzalez, J. A. Rodríguez and C. Theoduloz, *Bioorg. Med. Chem.*, 2008, **16**, 10172–10181.
4 S. I. Alqasoumi, A. M. Al-Taweel, A. M. Alafeefy, E. Noaman and M. M. Ghorab, *Eur. J. Med. Chem.*, 2010, **45**, 738–744.
5 V. Nair, G. Chi, Q. Shu, J. Julander and D. F. Smee, *Bioorg. Med. Chem. Lett.*, 2009, **19**, 1425–1427.
6 V. Alagarsamy, *Pharmazie*, 2004, **59**, 753–755.
7 A. B. A. El-Gazzar, H. N. Hafez and G. A. M. Nawwar, *Eur. J. Med. Chem.*, 2009, **44**, 1427–1436.
8 V. Alagarsamy, R. Venkatesaperumal, S. Vijayakumar, T. Angayarkanni, P. Pounammal, S. Senthilganesh and S. Kandeeban, *Pharmazie*, 2002, **57**, 306–307.
9 H. Ghafuri, M. Zargari and A. Emami, *Asian J. Green Chem.*, 2023, **7**, 54–69.
10 M. kidwai, P. Dwivedi and A. Jahan, *J. Appl. Organomet. Chem.*, 2023, **3**, 156–168.
11 B. Baghernejad and M. Fiuzat, *J. Med. Nanomater. Chem.*, 2023, **5**, 235–242.
12 A. R. Moosavi-Zare, M. A. Zolfigol, E. Noroozizadeh, O. Khaledian and B. S. Shaghasemi, *Res. Chem. Intermed.*, 2016, **42**, 4759–4772.
13 A. R. Moosavi-Zare, M. A. Zolfigol, E. Noroozizadeh, M. Zarei, R. Karamian and M. Asadbegy, *J. Mol. Catal. A: Chem.*, 2016, **425**, 217–228.
14 M. A. Zolfigol, S. Baghery, A. R. Moosavi-Zare and S. M. Vahdat, *J. Mol. Catal. A: Chem.*, 2015, **409**, 216–226.
15 A. R. Moosavi-Zare, M. A. Zolfigol and A. Mousavi-Tashar, *Res. Chem. Intermed.*, 2016, **42**, 7305–7312.
16 F. Jalili, M. Zarei, M. A. Zolfigol, S. Rostamnia and A. R. Moosavi-Zare, *Microporous Mesoporous Mater.*, 2020, **294**, 109865–109897.
17 A. R. Moosavi-Zare and R. Najafi, *Sci. Rep.*, 2023, **13**, 16501–16510.
18 S. Esmaili, A. R. Moosavi-Zare and A. Khazaei, *RSC Adv.*, 2022, **12**, 5386–5394.
19 A. Zare, M. Dianat and M. M. Eskandari, *New J. Chem.*, 2020, **44**, 4736–4743.
20 A. Zare and M. A. Dianat, *Z. Naturforsch.*, 2021, **76**, 85–90.
21 F. Shirini, M. S. N. Langarudi, N. Daneshvar, N. Jamasbi and M. Irankhah-Khanghah, *J. Mol. Struct.*, 2018, **1161**, 366–382.
22 F. Osanlou, F. Nemati and S. Sabaqian, *Res. Chem. Intermed.*, 2017, **43**, 2159–2174.
23 A. Gholami, M. Mokhtary and M. Nikpassand, *Appl. Organomet. Chem.*, 2020, **34**, e6007.

24 A. Zare, N. Lotfifar and M. Dianat, *J. Mol. Struct.*, 2020, **1211**, 128030.
25 D.-Q. Shi, S.-N. Ni, F. Yang, J.-W. Shi, G.-L. Dou, X.-Y. Li, X.-S. Wang and S.-J. Ji, *J. Heterocycl. Chem.*, 2008, **45**, 693.
26 A. M. Rad and M. Mokhtary, *Int. Nano Lett.*, 2015, **5**, 109–123.
27 I. M. Moghaddampour, F. Shirini and M. S. N. Langarudi, *J. Mol. Struct.*, 2021, **1226**, 129336–129347.
28 O. G. Jolodar, F. Shirini and M. Seddighi, *Chin. J. Catal.*, 2017, **38**, 1245–1251.
29 S. Esmaili, A. R. Moosavi-Zare, A. Khazaei and Z. Najafi, *ACS Omega*, 2022, **7**, 45314–45324.
30 S. C. Azimi, *Iran. J. Catal.*, 2014, **4**, 113–120.
31 A. Zare and M. Barzegar, *Res. Chem. Intermed.*, 2020, **46**, 3727–3740.
32 K. R. Khillare, D. S. Aher, L. D. Chavan and S. G. Shankarwar, *RSC Adv.*, 2021, **11**, 33980.
33 F. Nemati and R. Saeedirad, *Chin. Chem. Lett.*, 2013, **24**, 370–372.
34 F. Shirini, M. S. N. langarudi, N. Daneshvar, M. Mashhadinezhad and N. Nabinia, *J. Mol. Liq.*, 2017, **243**, 302–312.
35 A. R. Moosavi-Zare, H. Goudarziafshar and Z. Bahrami, *Res. Chem. Intermed.*, 2023, **49**, 507–523.
36 A. Zare, M. Barzegar and A. R. Moosavi-Zare, *Iran. J. Catal.*, 2024, **14**, 1–11.
37 S. Momeni and R. Ghorbani-Vaghei, *Sci. Rep.*, 2024, **14**, 21531–215317.
38 Z. Jalilian, A. R. Moosavi-Zare and M. Ghadermazi, *Res. Chem. Intermed.*, 2025, **51**, 2415–2433.
39 K. Tabatabaeian, A. F. Shojaei, F. Shirini, S. Z. Hejazi and M. Rassa, *Chin. Chem. Lett.*, 2014, **25**, 308–312.
40 D.-Q. Shi, L.-H. Niu, H. Yao and H. Jiang, *J. Heterocycl. Chem.*, 2009, **46**, 237–242.
41 P. Salehi, M. Dabiri, M. A. Zolfigol and M. A. B. Fard, *Tetrahedron Lett.*, 2003, **44**, 2889–2891.
42 S. Hamoudi and S. Kaliaguine, *Microporous Mesoporous Mater.*, 2003, **59**, 195–204.
43 S. Esmaili, A. Khazaei, A. Ghorbani-Choghamarani and M. Mohammadi, *RSC Adv.*, 2022, **12**, 14397–14410.
44 M. L. Testa and V. L. Parola, *Catalysts*, 2021, **11**, 1143.
45 A. R. Moosavi-Zare, H. Afshar-Hezarkhani and M. M. Rezaei, *Polycyclic Aromat. Compd.*, 2020, **40**, 150–158.
46 A. R. Moosavi-Zare, M. A. Zolfigol, V. Khakyzadeh, C. Böttcher, M. H. Beyzavi, A. Zare, A. Hasaninejad and R. Luque, *J. Mater. Chem. A*, 2014, **2**, 770–777.
47 A. R. Moosavi-Zare, M. A. Zolfigol, F. Derakhshan-Panah and S. Balalaie, *Mol. Catal.*, 2018, **449**, 142–151.
48 M. A. Zolfigol, A. Khazaei, A. R. Moosavi-Zare, A. Zare and V. Khakyzadeh, *Appl. Catal., A*, 2011, **400**, 70–81.
49 A. R. Moosavi-Zare, M. A. Zolfigol, M. Zarei, A. Zare, V. Khakyzadeh and A. Hasaninejad, *Appl. Catal., A*, 2013, **467**, 61–68.
50 M. Zarei, E. Noroozizadeh, A. R. Moosavi-Zare and M. A. Zolfigol, *J. Org. Chem.*, 2018, **83**, 3645–3650.
51 E. Abbasi, M. Milani, S. F. Aval, M. Kouhi, A. Akbarzadeh, H. T. Nasrabadi, P. Nikasa, S. W. Joo, Y. Hanifepour, K. Nejati-Koshki and M. Samiei, *Crit. Rev. Microbiol.*, 2016, **42**, 173–180.
52 X. Zhang, Z. Qu, X. Li, M. Wen, X. Quan, D. Ma and J. Wu, *Sep. Purif. Technol.*, 2010, **72**, 395–400.
53 V. V. Dutov, G. V. Mamontov, V. I. Zaikovskii, L. F. Liotta and O. V. Vodyankina, *Appl. Catal., B*, 2018, **221**, 598–609.
54 S. Lambert, C. Cellier, E. M. Gaigneaux, J.-P. Pirard and B. Heinrichs, *Catal. Commun.*, 2007, **8**, 1244–1248.
55 T. Ung, L. M. Liz-Marzán and P. Mulvaney, *J. Phys. Chem. B*, 1999, **103**, 6770–6773.
56 Y. Cao, W.-L. Dai and J.-F. Deng, *Appl. Catal., A*, 1997, **158**, L27–L34.
57 S. V. Otari, H. M. Yadav, N. D. Thorat, R. M. Patil, J. K. Lee and S. H. Pawar, *Mater. Lett.*, 2016, **167**, 179–182.
58 A. Naydenov, P. Konova, P. Nikolov, F. Klingstedt, N. Kumar, D. Kovacheva, P. Stefanov, R. Stoyanova and D. Mehandjiev, *Catal. Today*, 2008, **137**, 471–474.
59 I. Y. Ahn, J. H. Lee, S. K. Kim and S. H. Moon, *Appl. Catal., A*, 2009, **360**, 38–42.
60 Y. Shi, X.-L. Zhang, G. Feng, X. Chen and Z.-H. Lu, *Ceram. Int.*, 2015, **41**, 14660–14667.
61 M. Guo, J. Ding, G. Ji, T. Xie, H. Pang, X. Li and Q. Zhong, *Mol. Catal.*, 2024, **556**, 113898.
62 B. Zhao, Z. Dong, Q. Wang, Y. Xu, N. Zhang, W. Liu, F. Lou and Y. Wang, *Nanomaterials*, 2020, **10**, 883.
63 C. V. Khedkar, K. D. Daware, P. S. Badgujar, Y. D. Kolekar, S. W. Gosavi and S. I. Patil, *Opt. Mater.*, 2021, **120**, 111426.
64 Z. Luo, Y. Shen, D. Fang, C. He, Y. Cao, W. Li, Y.-A. Zhu, J. Zhou and X. Zhou, *Mol. Catal.*, 2024, **559**, 114109.
65 H. Chen, J. Tan, J. Cui, X. Yang, H. Zheng, Y. Zhu and Y. Li, *Mol. Catal.*, 2017, **433**, 346–353.
66 S. Cheng, D. Mao, X. Guo and J. Yu, *React. Kinet. Mech. Catal.*, 2019, **126**, 1067–1079.
67 C. E. Volckmar, M. Bron, U. Bentrup, A. Martin and P. Claus, *J. Catal.*, 2009, **261**, 1–8.
68 J. Chen, Z.-H. Lu, Y. Wang, X. Chen and L. Zhang, *Int. J. Hydrogen Energy*, 2015, **40**, 4777–4785.
69 I. Y. Ahn, J. H. Lee, S. K. Kim and S. H. Moon, *Appl. Catal., A*, 2009, **360**, 38–42.
70 R. Wojcieszak, S. Monteverdi, J. Ghanbaja and M. M. Bettahar, *J. Colloid Interface Sci.*, 2008, **317**, 166–174.
71 Y. Hai, T. Guan, Y. Feng, Z. Zhen, Y. Yang, Y. Hu, J. Lv, Y. Wang and X. Ma, *Chem. Eng. Sci.*, 2024, **294**, 120121.
72 R. M. Mourad, O. M. Darwesh and A. Abdel-Hakim, *Int. J. Biol. Macromol.*, 2020, **164**, 3243–3249.
73 R. Heydari and M. Rashidipour, *Int. J. Breast Cancer*, 2015, **6**, 846743.
74 R. S. Priya, D. Geetha and P. S. Ramesh, *Ecotoxicol. Environ. Saf.*, 2016, **134**, 308–318.
75 M. Malekzadeh, K. L. Yeung, M. Halali and Q. Chang, *Mater. Sci. Eng. C*, 2019, **102**, 616–622.
76 C. D. Wagner, The NIST X-Ray photoelectron seectroscopy (XPS) database, 1991.

77 Y.-C. Wang, M. H. Engelhard, D. R. Baer and D. G. Castner, *Anal. Chem.*, 2016, **88**, 3917–3925.
78 B. Zamani-Ranjbar-Garmroodi, M. A. Nasseri, A. Allahresani and K. Hemmat, *Res. Chem. Intermed.*, 2019, **45**, 5665–5680.
79 G. B. Park, B. S. Singu, S. E. Hong and K. R. Yoon, *Bull. Korean Chem. Soc.*, 2016, **37**, 1501–1508.
80 Y. H. Kim, D. K. Lee and Y. S. Kang, *Colloids Surf., A*, 2005, **257–258**, 273–276.
81 K. Mohammadi, F. Shirini and A. Yahyazadeh, *RSC Adv.*, 2015, **5**, 23586–23590.